Aminopropyl-modified mesoporous silica nanospheres for the adsorption of Cr(VI) from water

N. Fellenz, P. Martin, S. Marchetti & F. Bengoa

Journal of Porous Materials

ISSN 1380-2224
Volume 22
Number 3

J Porous Mater (2015) 22:729-738
DOI 10.1007/s10934-015-9946-4

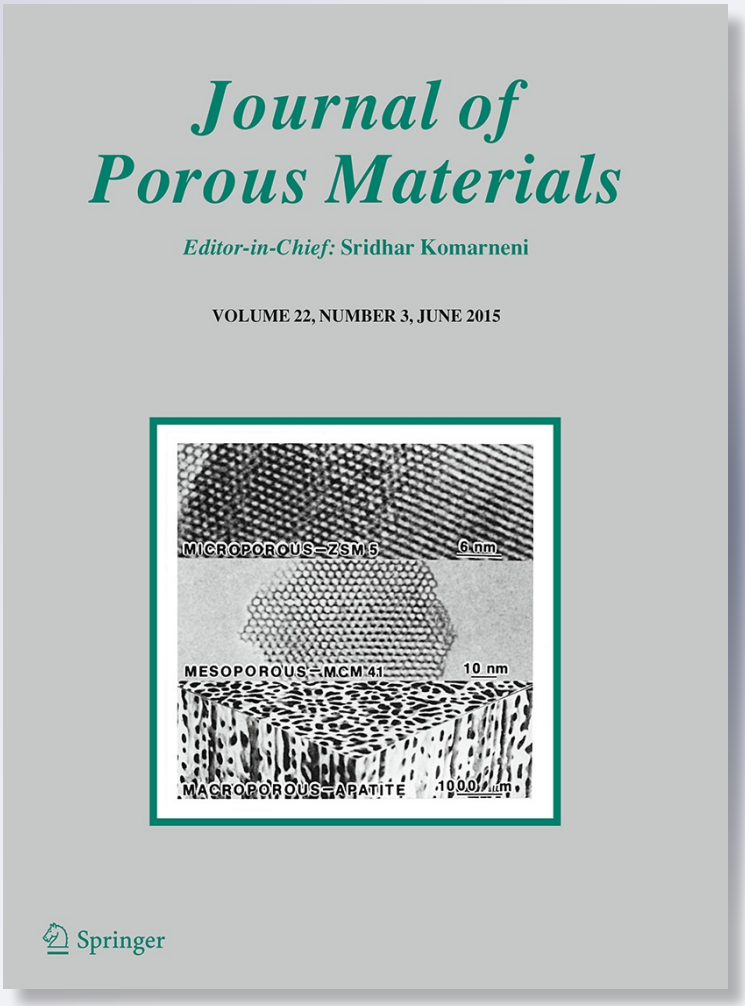

Springer

Your article is protected by copyright and all rights are held exclusively by Springer Science +Business Media New York. This e-offprint is for personal use only and shall not be self-archived in electronic repositories. If you wish to self-archive your article, please use the accepted manuscript version for posting on your own website. You may further deposit the accepted manuscript version in any repository, provided it is only made publicly available 12 months after official publication or later and provided acknowledgement is given to the original source of publication and a link is inserted to the published article on Springer's website. The link must be accompanied by the following text: "The final publication is available at link.springer.com".

Author's personal copy

J Porous Mater (2015) 22:729–738
DOI 10.1007/s10934-015-9946-4

Aminopropyl-modified mesoporous silica nanospheres for the adsorption of Cr(VI) from water

N. Fellenz[1] · P. Martin[1] · S. Marchetti[2] · F. Bengoa[2]

Published online: 19 March 2015
© Springer Science+Business Media New York 2015

Abstract Aminopropyl-functionalized mesoporous silica spherical particles were obtained through post-synthetic route. The suitability of this material as an adsorbent for heavy metals from aqueous media was tested by Cr(VI) adsorption experiments performed at various pH conditions, chromium concentrations and time. The synthesized particles were characterized before and after functionalization by X-ray diffraction at low angles, nitrogen adsorption–desorption isotherms, infrared Fourier transform spectroscopy, scanning electron microscopy and thermogravimetric analysis. It was found that Cr(VI) adsorption occurs more efficiently in the pH range between 2 and 3. As a consequence of the nanometer scale of the particles, concentration profiles do not develop inside of them and thus there are no diffusional restrictions within the pores, leading to a higher Cr(VI) adsorption than that previously reported for similar systems. Chromium desorption for material reutilization was carried out in basic media. Results showed that the amino groups were grafted successfully without mesostructure damage. These groups are essential for the metal ion removal and no significant leaching was observed after four use/regeneration/use cycles. The batch equilibrium data fitted well the Langmuir isotherm with a maximum adsorption capacity of 87.1 mg g^{-1} at 25 °C. A discussion about the relationship between structure and its behavior as adsorbent, including regeneration and reusability, is given.

Keywords Ordered mesoporous silica · Spherical particles · Amino-functionalization · Adsorption · Hexavalent chromium

1 Introduction

Population growth and the industrial activity associated with it generate large amounts of wastes and effluents containing different organic and inorganic pollutants [1]. Thus, in the last decades a growing level of pollution has been recorded in the different sources of drinking water. Heavy metals are among the most important contamination sources, and especially the chromium as it has high mutagenesis capability even at very low concentrations. The main industrial sources of Cr(VI) are: alloys and steel manufacturing, metal finishing, electroplating, leather tanning, and pigments synthesis and dyeing. For these reasons, considerable efforts have been made to develop new processes and materials for industrial wastewater treatment, recovery of pollutant species and remediation of the affected water sources. Adsorption is one of the most frequently used techniques [2, 3], with a great number of materials being tested as adsorbents. The materials that have been studied so far include: natural or synthetic solids [4, 5], clays or mixed hydroxides [6, 7], metal oxides [8], natural organic matter [9], bioadsorbents (bacterium, algae and fungi) [10], advanced material such as functional polymers, organic/inorganic hybrid structures [11–13], etc. Among them, organic/inorganic hybrid materials based on ordered mesoporous silicas (OMS) are more useful than

Electronic supplementary material The online version of this article (doi:10.1007/s10934-015-9946-4) contains supplementary material, which is available to authorized users.

✉ F. Bengoa
bengoajf@quimica.unlp.edu.ar

[1] Universidad Nacional de Rio Negro, CONICET, Belgrano 526, 8500 Viedma, Rio Negro, Argentina

[2] Departamento de Química, Facultad de Ciencias Exactas, Universidad Nacional de La Plata, CONICET, CINDECA, CICPBA, 47 No 257, 1900 La Plata, Argentina

Author's personal copy

other materials since they exhibit high specific surface areas and narrow pore size distributions [14, 15]. Moreover, these OMS-based hybrid materials provide both a high-thermal stability, due to the SiO_2 three-dimensional network, and a specific surface chemical reactivity, determined by the different organic functions that can be added to the surface [16]. There are two routes for the incorporation of organic functions onto OMS solids, i.e., the co-condensation route and the post-synthesis or post-grafting method. The selected method clearly affects the textural and chemical properties of the final hybrid silica material and thus its performance as adsorbent [17]. This is mainly because when co-condensation is used, up to 80 % of the organic groups may be incorporated within the walls of the mesoporous matrix and therefore they are inaccessible for the adsorbate [18]. When the post-synthesis method is chosen, a complete exposure of the organic functions can be achieved [19].

Several kinds of organically modified OMS have been used for adsorption of heavy metals ions. The results show a high separation capacity for these adsorbents and the possibility of being regenerated and reused repeatedly [20–23]. Besides, both the macrostructure morphology and the size of the adsorbent particles have been found to affect the behavior in the separation process [24, 25]. Therefore, it is important to study the synthesis and evaluation of these materials (e.g. defined morphology, accessible functional groups, long-term stability) and their adsorptive capacity towards heavy metals. Among the mesoporous silica materials, MCM-41, which has a hexagonal mesopores arrangement, is an ideal candidate for designing general purpose adsorbents once modified with organic groups, because it can be obtained from an inexpensive source such as rice husk [26].

The aim of this work is to study the Cr(VI) adsorption on nanometer spherical mesoporous MCM-41 particles in order to avoid diffusional effects. The synthesis and characterization of aminopropyl-modified MCM-41 nano spheres using the post-synthetic surface modification route are reported. Cr(VI) adsorption onto the resulting material was evaluated and the effect of pH, time and metal concentration on the adsorption was studied. Desorption in basic media was carried out to study adsorbent regeneration.

2 Materials and methods

2.1 Synthesis of mesoporous silica spherical particles

Ordered mesoporous silica spheres were prepared following the methodology proposed by Grün et al. [27] using tetraethyl orthosilicate (TEOS, ≥99 %, Aldrich) as silica source, n-hexadecyltrimethylamonnium bromide (CTMABr, ≥98 %, Sigma) as structure-directing agent, distilled water, absolute ethanol (Cicarelli, 99.5 %) and NH_4OH (28 % p/p) to generate an alkaline medium. To obtain ≈2.5 g of solid product, 100 mL of distilled water, 60 mL of NH_4OH, 5 g of CTMABr, 150 mL of absolute ethanol and 10 mL of TEOS were mixed under vigorous magnetic stirring. The synthesis gel has the following molar composition: $1TEOS:0.3CTMABr:11NH_4OH:58ethanol:144H_2O$. The reaction mixture was kept under stirring at room temperature (30 °C) for 2 h. The white precipitate was collected by filtration and washed with distilled water. To remove the CTMABr the sample was calcined up to 550 °C in air atmosphere for 2 h, with a heating rate of 10 °C min^{-1}. The final sample obtained was called MSSP.

2.2 MSSP aminopropyl-functionalization

Two aminopropyl-functionalized hybrid materials were obtained by post-synthetic treatment of MSSP using 3-Aminopropyltriethoxysilane (APTES, ≥98 % Sigma) in toluene. For this purpose, 1.5 g of MSSP were dispersed in 150 mL of toluene and heated at 80 °C under intense magnetic stirring. Later 1.5 g of APTES ($\delta = 0.989$ cm^3 g^{-1}) was added and the mixture was stirred at 80 °C for 6 h. After this period the solid product was separated by Buchner filtration and washed four times with 50 mL of ethanol and four times with 50 mL of water. The aminopropyl-modified sample was called MSSP-APS. A fraction of this sample was treated with water under magnetic stirring at T = 30 °C for 24 h, with a solid/water ratio equal to 1 g L^{-1}. The resulting solid was filtered on Buchner and dried at 100 °C. This sample, extensively washed, was named MSSP-APSw.

2.3 Sample characterization

The solids were characterized before and after functionalization by X-ray diffraction (XRD) at low angles, N_2 adsorption–desorption at −196 °C, infrared spectroscopy (FT-IR), thermo-gravimetric analysis (TGA) and scanning electron microscopy (SEM).

All X-ray diffraction patterns at low angles were recorded using a standard automated powder X-ray diffraction system (Philips PW 1710) with diffracted-beam graphite monochromator using Cu K_α radiation ($\lambda = 1.54056$ A) in the range $2\theta = 1.5°–8°$ with steps of 0.02° and counting time of 2 s/step.

The N_2 adsorption–desorption isotherms were obtained in a Micromeritics equipment ASAP 2020 V1.02 E. The surface area was estimated by the Brunauer–Emmet–Teller (BET) method and the total pore volume was obtained at $P/P_0 = 0.99$ using the Gurvich method. The pore size

Author's personal copy

distribution was determined by the Barrett–Joyner–Halenda/Kruk–Jaroniec–Sayari (BJH-KJS) method from the adsorption branch of the isotherm [28].

The FT-IR absorption spectra were acquired with a Bruker IFS66 spectrometer with 1 cm^{-1} resolution by co-addition of 32 scans. The samples were mixed with potassium bromide (1:100 proportion) in order to obtain the corresponding pellets.

A Philips 505 microscope was used for SEM analysis. The TGA measurements were performed on a Shimadzu TGA-50 apparatus. The sample was heated from room temperature to 750 °C at a heating rate of 5 °C min^{-1} under air flow (20 cm^3 min^{-1}).

2.4 Chromium adsorption experiments

A stock solution of Cr(VI) (1500 ppm) was prepared using distilled water and the primary standard $K_2Cr_2O_7$ (Cicarelli, reagent grade). All the Cr(VI) solutions used in the present work were obtained by diluting this primary solution using a precision variable volume single pipette (range 1000–2500 ± 12 µl). In all cases batch-like experiments were realized under magnetic stirring (500 rpm) with 25 ml of chromium solution at the desired initial concentration and 25 mg of fresh adsorbent. The temperature for all tests was 25 ± 2 °C.

Cr(VI) uptake was investigated as a function of time by performing experiments at different pH at 25 °C. To that end, 25 mg of adsorbent were suspended under magnetic stirring in 25 ml of 10 ppm Cr(VI) aqueous solution with the selected pH value. These experiments were conducted in duplicate at constant pH values of 2.2, 3.5, 5.1 (±0.2). In all the cases the desired pH value was adjusted by adding a small amount (one or two drops) of concentrated hydrochloric acid solution at the beginning of the experiment and, if necessary, during the test. In addition, an experiment was conducted by adding the solid sample to a 10 ppm chromium solution without HCl, in this case the initial pH was 5.1. This last assay was called test without pH control.

To obtain the adsorption isotherm at 25 °C, experiments were carried out with 25 mg of adsorbent kept in suspension by magnetic stirring in 25 ml of solution. Different initial chromium concentrations in the range 10–130 ppm (obtained by dilution of the stock solution as previously explained), with constant pH equal to 2.2 (±0.2) adjusted using HCl and contact time of 24 h were studied. In order to diminish the experimental error, each experiment was performed twice using fresh solid each time. Due to the fact that adsorption velocity of Cr(VI) is high, as previously reported for different solids [7, 9, 11] and will be further discussed with the results of the present work, it was assumed that at the end of this period of time equilibrium was attained. In all the experiments, after adsorption, the solids were separated by filtration and the residual chromium concentration in the supernatant was determined by visible–UV spectroscopy at 540 nm using the method of 1,5 diphenylcarbazide [29]. Details of this technique are shown in Supporting Information Section. The percentage of chromium removed, R, was calculated by the following equation: $R(\%) = (C_0 - C_t)/C_0 \times 100$ %, where C_0 is the initial Cr(VI) concentration, and C_t is the concentration at time t or at equilibrium (24 h).

2.5 Chromium desorption and reutilizationand stability of the mesoporous hybrid material

Desorption was performed under basic conditions. The used hybrid material (with adsorbed chromium) was immersed into a NaOH solution (pH 8) and stirred for 60 min. The regenerated solid was separated by filtration, dried and was reused in a new adsorption test performed as described above (pH = 2.2 and 10 ppm of chromium). This adsorption/desorption cycle was repeated four times to evaluate the long term reusability of the synthesized particles.

To test the stability of the mesoporous hybrid material, the aminopropyl leaching in aqueous media, which emulates the desorption process, was measured. For this purpose, 100 mg of APS sample was contacted 50 ml of basic solution (pH 8) and stirred over 240 min. After that, the sample was separated by filtration and the amino groups in solution were determined by titration using HCl 0.1 M as it was described in literature [30].

3 Results and discussion

3.1 Solid characterization

Figure 1 shows the SEM images of particles from which the size distributions were obtained, considering 150 particles for each sample (Fig. 2). The distributions were fitted using a gauss function. It can be seen that all samples are composed of spherical particles (Fig. 1a- for MSSP, b- for MSSP-APS and c- for MSSP-APSw). The diameter (arithmetic mean) is equal to 459 ± 11, 487 ± 10 and 467 ± 6 nm and the estimated width at half height (FWHM) is 280, 238 and 250 nm for MSSP, MSSP-APS and MSSP-APSw respectively.

Figure 3 shows the XRD patterns at low angles for the MSSP, MSSP-APS and MSSP-APSw. In all diffractograms a narrow main peak is observed at $2\theta = 2.6°$, and for sample MSSP two wide peaks with lower intensity, between 4° and 6°, are also visible. These diffraction patterns are characteristic of the ordered mesoporous materials and in our case is associated with a hexagonal arrangement of mesopores characteristic of MCM-41 material [14]. For

Author's personal copy

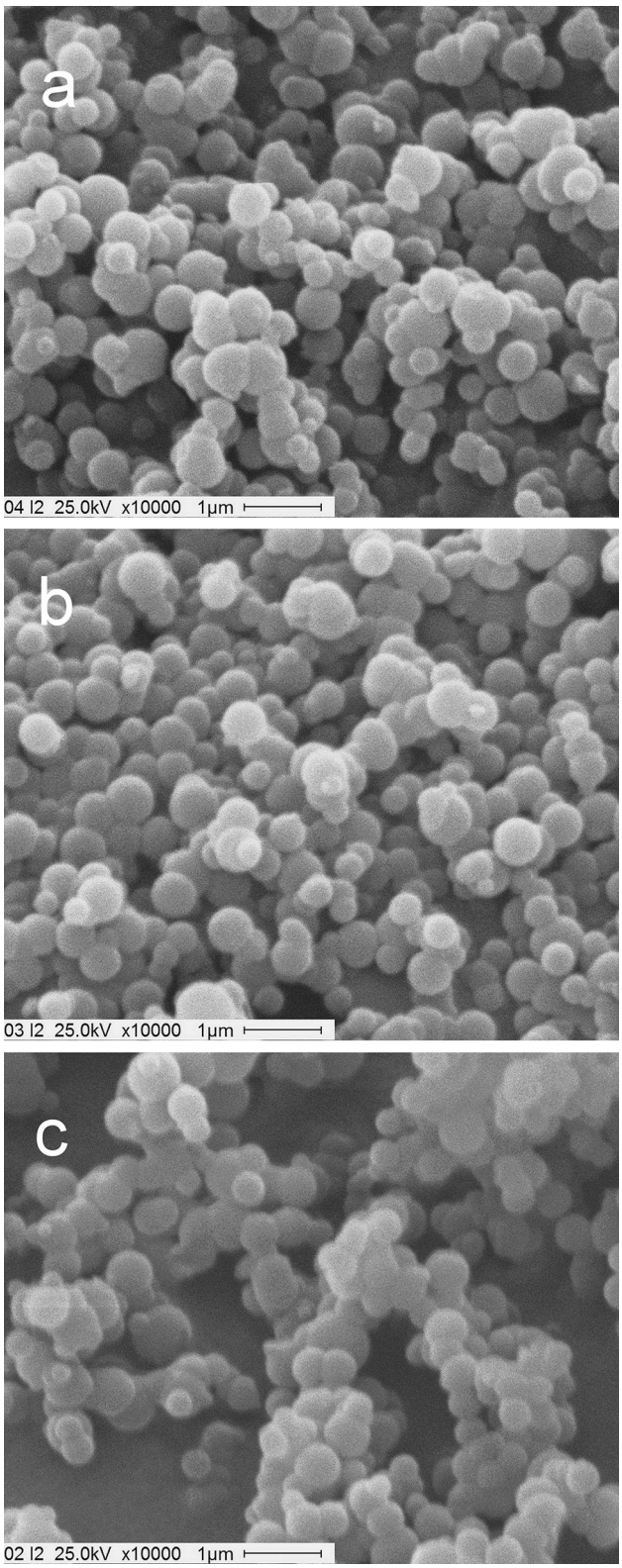

Fig. 1 SEM images of (**a**) MSSP, (**b**) MSSP-APS and (**c**) MSSP-APSw

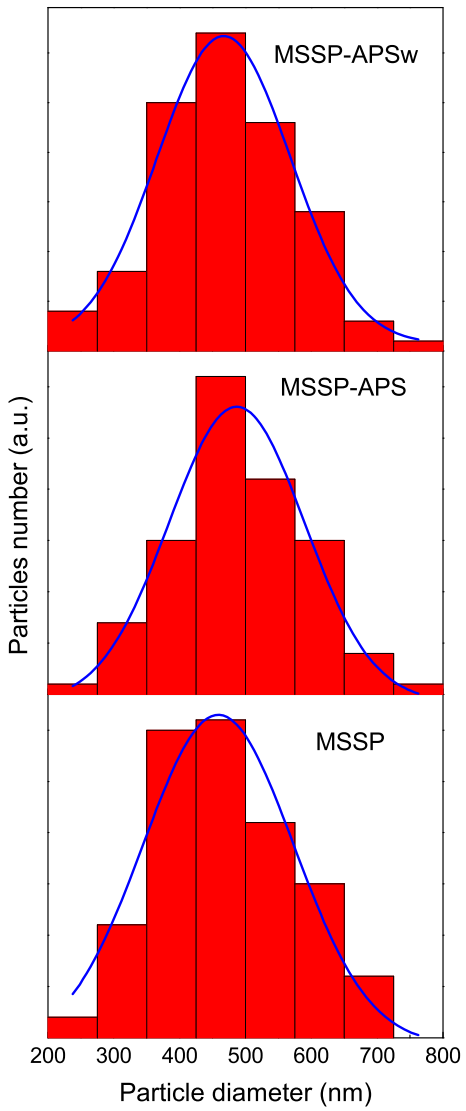

Fig. 2 Particle size distribution of MSSP, MSSP-APS and MSSP-APSw from SEM measurements (*lines* were obtained fitting the results by assuming a gauss distribution)

example, the interplanar distance for sample MSSP were: $d_{100} = 3{,}4$ nm, $d_{110} = 2.0$ nm, $d_{200} = 1.8$ nm. However, a decrease in the intensity of the diffraction peaks of the functionalized samples (APS samples) is observed. This was reported previously for amino grafted OMS materials obtained by the post-synthetic method, and was associated with two different phenomena: a partial structure damage of the ordered mesophase [24, 31] or a contrast matching between the inorganic SiO_2 framework and the grafted organic groups [19]. Surprisingly, the reduction in the main diffraction peak is more marked in the sample MSSP-APS than in MSSP-APSw. Further discussion of this behavior is

Author's personal copy

given below, with the analysis of the textural properties obtained from the nitrogen adsorption–desorption experiments and the TGA measurements.

To corroborate if the organic groups were incorporated covalently to the mesoporous structure, FT-IR measurements were conducted (Fig. 4). The spectrum of MSSP shows two bands at 1090 and 810 cm^{-1} which can be assigned to antisymmetric and symmetric stretching of the Si–O-Si species respectively [32]. Additional bands were observed in the aminofunctionalized samples at 690, 1470 and 1560 cm^{-1}, which can be attributed to the presence of amino groups [32, 33]. The band corresponding to the surface Si–OH stretching at 960 cm^{-1} becomes a shoulder in the APS samples when compared with MSSP spectrum, indicating that the presence of the amino groups reduce to some extent the amount of Si–OH species on the surface [32]. Therefore, these results indicate that in APS samples aminopropyl groups are covalently attached. It is important to remark that the aminopropyl groups incorporation onto OMS materials is frequently carried out using an APTES-toluene solution at its boiling point ($\approx$ 110 °C). Taking into account our FT-IR results jointly with the Cr(VI) adsorption data discussed bellow, it is demonstrated that is not necessary to use higher temperatures than $\approx$80 °C to get a covalently attach of aminopropyl groups onto MCM-41 surface. Higher temperatures lead to an unnecessary waste of energy, and also increase the possibility of damaging the mesostructure of the primary silica matrix.

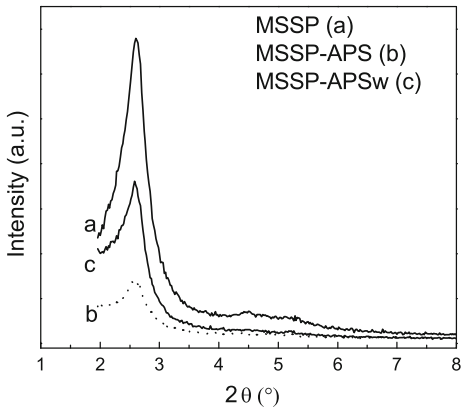

Fig. 3 XRD patterns at low angles of pure and hybrid materials

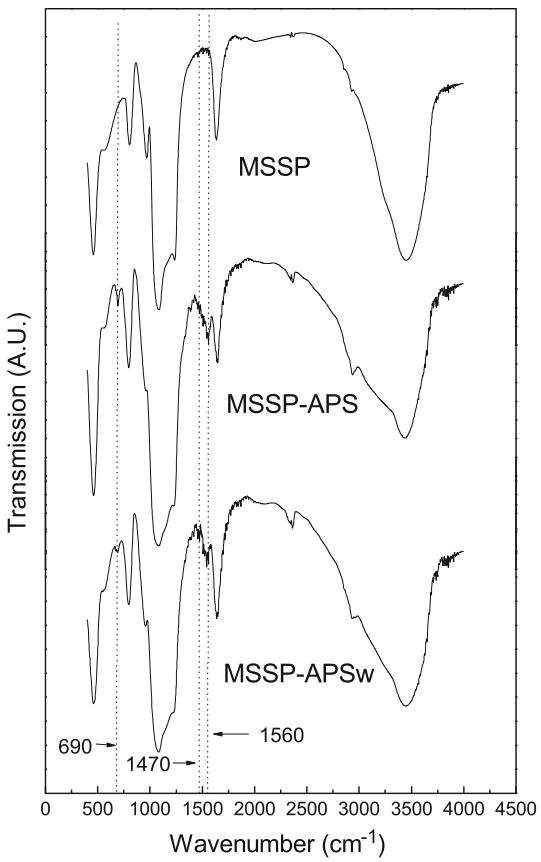

Fig. 4 FT-IR spectra of MSSP, MSSP-APS and MSSP-APSw

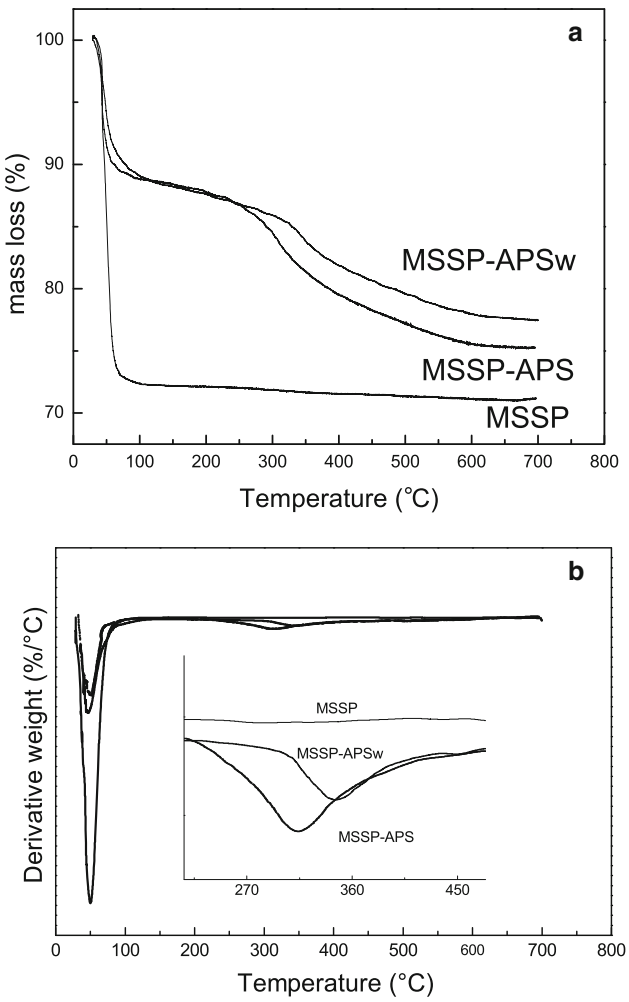

Fig. 5 Thermogravimetric analysis (**a**) and first derivative curve (DTG) (**b**)

Author's personal copy

Figure 5 shows the TGA and the first derivative (1st DTG) curves for the amino-functionalized and pure OMS samples. The loss of mass observed at low temperature is produced by desorption of physisorbed water molecules on the solid, a process that ends at ≈130 °C. The functionalized samples present a second peak, which is much higher than for MSSP, and can be ascribed to the elimination of the aminopropyl grafted groups [31, 34, 35]. For MSSP-APS this second peak, starts at about 220 °C, while for MSSP-APSw it appears at about 300 °C, ending in all samples at approximately 650 °C. Since condensation of silanols groups (dehydroxylation) occurs in this range of temperature it would be not possible, using this technique, determine accurately the number of aminopropyl groups anchored on the functionalized samples. However, taking into account that the mass loss due to the dehydroxylation of MSSP is much lower than that of the functionalized samples (Fig. 5b), a rough estimation can be made.

The values calculated with these assumptions were of 14 % for MSSP-APS and 9 % for MSSP-APSw respectively. As it was established above, the degradation of the aminopropyl groups present in MSSP-APS starts at a lower temperature than for MSSP-APSw sample [220 vs. 300 °C, Fig. 5b (inset)]. Considering that the boiling point for pure APTES is 226 °C, this last difference suggests that there are two kinds of aminopropyl groups present in MSSP-APS. The first one is physisorbed on the surface of the mesopores; therefore, when temperature increases these groups have a very similar behavior to pure APTES. The second one is covalently bonded to the surface of the mesoporous structure. This result indicates that a simple wash after the post-synthesis surface modification is not enough to remove the physisorbed, unreacted APTES, while they are completely removed after immersing the sample in water during 24 h under stirring.

Taking into account the previous discussion, the difference in XRD intensities between the samples (Fig. 3) can be attributed to the different quantities of APTES and/or aminopropyl groups present in the samples. Thus, when the physisorbed APTES is removed, the intensity of the principal peak increases, meaning that the sample MSSP-APS did not suffer a damage of the mesostructure. Instead, the intensity diminution can be attributed to the filling of the mesoporous with APTES (physisorbed), which produces a decrease of the contrast in accordance with Mercier et al. [19].

Figure 6 shows the nitrogen adsorption–desorption isotherms at −196 °C, while Table 1 shows the values of the textural properties and the wall thickness for all samples. The wall thickness values were calculated using the Braggś equation and the mean pore diameter using a procedure described in literature [36]. The isotherms of the pure and amino modified samples show the characteristic shape of type IV curves according to the IUPAC classification, associated with mesoporous materials. The absence of a hysteresis loop is associated with a reversible adsorption–desorption process suggesting the presence of pores with diameters smaller than 4 nm [28, 37]. The point corresponding to capillary condensation takes place at low values of relative pressure; besides, a slight shifting towards lower P/P_0 is observed for MSSP-APSw sample indicating a reduction in the pores size caused by the post-synthesis treatment. This shift is much more pronounced for MSSP-APS. The specific surface area and total pore volume undergo a considerable reduction after surface modification (Table 1). The S_g reduction is noticeably higher for MSSP-APS (80 %) than for MSSP-APSw (23 %), and would imply an almost complete filling of the pores in MSSP-APS due to the presence of physisorbed APTES which may block the entrance of the pores. This is not observed in MSSP-APSw sample because the physisorbed APTES was removed after washing 24 h. Due to the poor porosity of MSSP-APS system, mean pore diameter determination, through the BJH-KJS method, and wall thickness were not possible to calculate.

Taking into account that the surface of MCM-41 is rich in silanol groups (Si–OH), the variations observed for MSSP-APSw can be partly explained considering the following scheme for the reaction between MSSP and APTES:

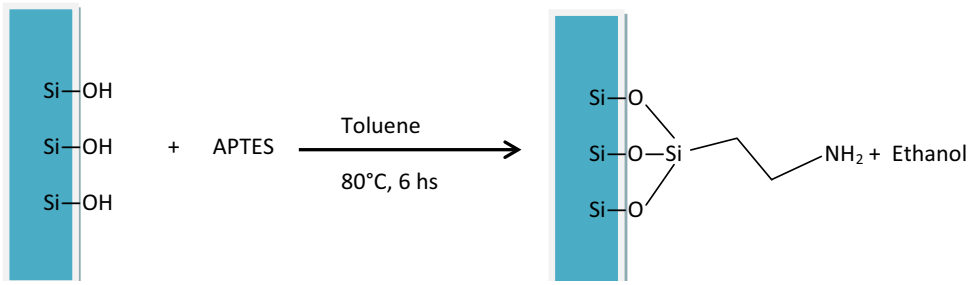

Author's personal copy

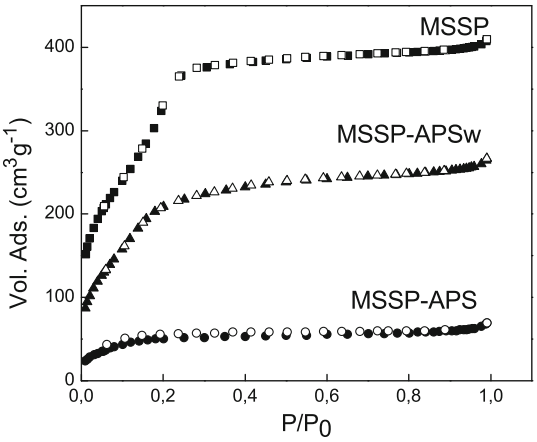

Fig. 6 Nitrogen adsorption (*full symbols*)-desorption (*empty symbols*) isotherms for MSSP, MSSP-APS and MSSP-APSw

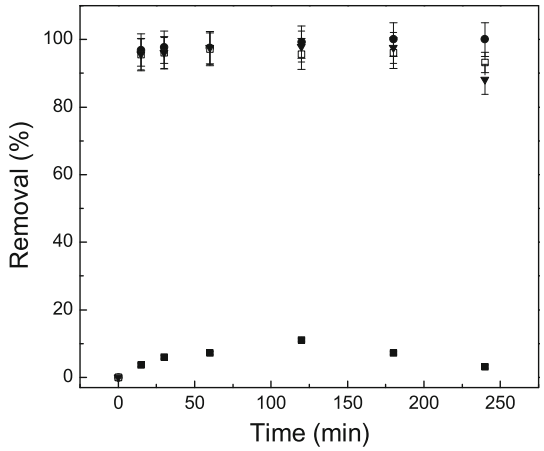

Fig. 7 Chromium removal (%) at different pH constant values as a function of time using 25 mg of adsorbent in 25 mL of 10 ppm chromium solution and 25 °C, *filled squares*: MSSP (pH 2.2) and MSSP-APSw *filled circles*: (pH 2.2), *open squares*: (pH 3.1), *filled inverted triangles*: (pH 5.1)

Table 1 Textural properties of MSSP, MSSP-APS and MSSP-APSw

	S_g^a (m^2 g^{-1})	V_p^b (cm^3 g^{-1})	D_p^c (nm)	E_{wall}^d (nm)
MSSP	1081	0.6	2.9	1.0
MSSP-APS	189	0.1	–	–
MSSP-APS-w	834	0.4	2.5	1.3

[a] Sg: specific surface area

[b] Dp: average pore diameter

[c] Vp: specific pore volume

[d] Ewall: wall thickness

However, the reduction in the mean pore diameter (Table 1) caused by the difference in sizes between the OH group and the aminopropyl group, cannot account for the total variations observed in S_g and V_p. Thus, in MSSP-APSw a small fraction of the pores might be occluded by anchorage of aminopropyl groups. Then, the variations in the textural properties in MSSP-APSw can be explained considering some hierarchical polymerization of the organosilane grafted groups that cause a partial blockage a some pores decreasing S_g and V_p. The latter explanation has been recently reported even for SBA-15 systems with pore diameters larger than 5 nm [20]. Finally, the wall thickness showed a slight increase for MSSP-APSw in comparison with MSSP, in agreement with the variation recorded in D_p as in can be seen in Table 1.

3.2 Chromium adsorption

Due to the poor porosity of the MSSP-ASP sample, this was not tested for adsorption experiments. All adsorption tests which will be mentioned hereafter were made with the MSSP-APSw sample.

The Cr(VI) adsorption kinetics at constant pH values of 2.2, 3.5 and 5.1 (±0.2) was determined with a Cr(VI) initial concentration of 10 ppm (Fig. 7). Fast adsorption velocity was observed, reaching 95 % removal in the first 15 min and keeping at approximately constant values throughout the whole period of time studied and in the whole pH range. A complete chromium removal was attained only when the pH was fixed externally at 2.2. No significant Cr(VI) adsorption takes places when MSSP was used as adsorbent material at pH = 2.2 (Fig. 7), indicating that the presence of surface amino groups generates the necessary sites for the interaction with the chromium species. Figure 8 shows the removal percentage at constant time (240 min) in the pH range of 2.2–7.1. The dependence with the pH of the adsorption capacity of the solids towards different metals is determined by two factors, the metal behavior in solution and acid–base characteristics of the solid surface. The behavior of Cr(VI) in aqueous solution can be described by the following equations, Eq. (1–3):

$$HCrO_4^- \leftrightarrow CrO_4^{2-} + H^+ \quad (pKa = 5.9) \tag{1}$$

$$H_2CrO_4 \leftrightarrow HCrO_4^- + H^+ \quad (pKa = 4.1) \tag{2}$$

$$Cr_2O_7^{2-} + H_2O \leftrightarrow 2\,HCrO_4^- \quad (pKa = 2.2) \tag{3}$$

Thus, at pHs between 2.2 and 5.9 and a Cr(VI) concentration equal to 10 ppm, the predominant species is $HCrO_4^-$ [7, 9]. On the other hand, in this range of pH almost all the surface amino groups of the adsorbent are in the ammonium form $–NH_3^+$ [38, 39]. Therefore, the small differences observed in the chromium uptake in the pH range of 2.2–5.1, displayed in Fig. 8, can be understood considering that a gradual loss of protons of the surface silanols (pKa ≈ 6–7) and a decrease in NH_3^+/NH_2 ratio take place as the pH increases [24, 38, 40].

Author's personal copy

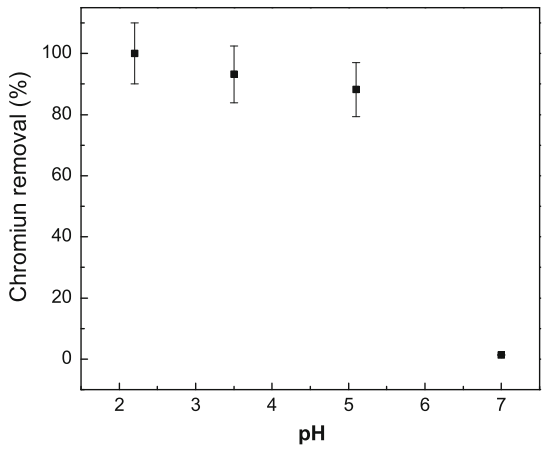

Fig. 8 Effect of pH in chromium removal (%) at constant time of 240 min for MSSP-APSw, 25 mg of adsorbent in 25 mL of 10 ppm chromium solution and 25 °C

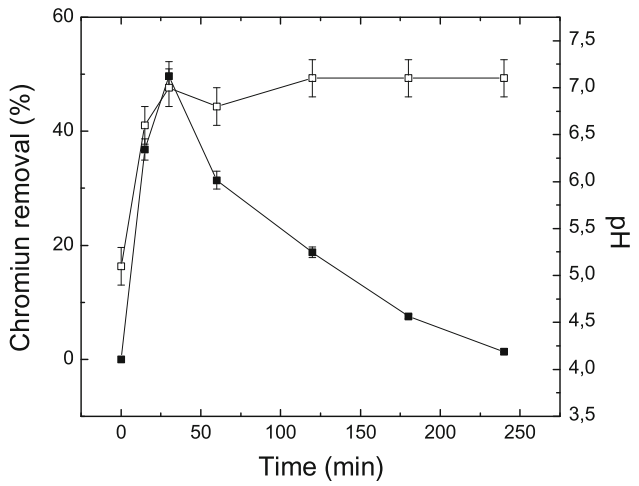

Fig. 9 MSSP-APSw free pH assay: chromium removal (%) (*filled squares*) and pH value variation (*open squares*) versus time

If the pH is not regulated externally, free pH assay, an increase from 5.1 to 7.1 in the pH value was observed and the kinetic adsorption shows a more complex behavior (Fig. 9) than in the experiments conducted at constant pH values. In the first 30 min the amount of Cr(VI) adsorbed increased gradually, while pH increases from its initial value to 7.1. After that time, desorption of the chromium initially adsorbed starts, up to the complete desorption. Walcarius et al. realized a detailed analysis of the rate of protonation on different OMS modified with amino groups [24]. They determined that the protonation in distillated water of ordered mesoporous organosilicas was extremely fast in the early times, with >80 % protonation in <2 s. So, in the early stage of the free pH assay, the Si-$C_3H_6NH_3^+$ species are produced very quickly and this generates the first suitable sites for chromium adsorption. As the pH increases gradually (Fig. 9, empty symbols) it promotes the CrO_4^{2-} formation and the gradual deprotonation of the ammonium and silanols surface species. Finally, when pH ≈ 7 the principal Cr(VI) specie is CrO_4^{2-} (80 %) while $HCrO_4^-$ is the minor one (20 %) [41]. At this stage the deprotonation of the remaining surface silanols is more pronounced, which generates a surface with some negative charges. In consequence, the silanolates species would repel the initially adsorbed chromium anions; an adsorbent/adsorbate repulsion takes place due to the negative charge of the chromium anion and the SiO^- species. This phenomenon was reported previously by other authors but dealing with positive charges [42]. In this case, they reported that the formation of positively charged complexes located on the internal walls of the porous material, acted as an electrostatic barrier, limiting the further penetration of large quantities of positively charged species.

In order to determine the maximum adsorption capacity of MSSP-APSw, the adsorption isotherm at 25 °C was obtained under equilibrium conditions (24 h) at pH 2.2, with initial concentrations of Cr(VI) between 10 and 130 ppm and adsorbent particle size of 467 ± 6 nm (Fig. 10a). The Langmuir monolayer model was used to fit the experimental data of the isotherm. The Langmuir isotherm can be linearized as shown in Eq. (4):

$$C_e/q_e = 1/K_L q_{max} + C_e/q_{max} \quad (4)$$

where q_{max} is the maximum adsorption capacity of the adsorbent in mg of adsorbate per g of adsorbent, K_L(L mg^{-1}) is the Langmuir constant which is related to the intensity of adsorbent/adsorbate interaction, q_e is the adsorbed amount in mg g^{-1} and C_e is the concentration of adsorbate in equilibrium in the solution expressed in mg L^{-1}. A correlation factor R^2 equal to 0.997 was obtained (Fig. 10b), indicating that this model represents properly the system under study. Therefore, a monolayer of $HCrO_4^-$ probably forms on the solid surface. A q_{max} value of 87 mg g^{-1} was found, which is higher than that reported for adsorbents composed of other solids such as modified activated carbons [11] and modified iron oxide magnetic nanoparticles [8, 43]. Cao et al. assessed an amino-functionalized MCM-41 for the adsorption of Cr(VI) at pH < 4, and the maximum adsorption capacity reported was 38.55 mg g^{-1} [22]. The controlled morphology, the small size of the adsorbent particles and their narrow size distribution present in our system, might be responsible for the difference found between both materials. Larger particle sizes could have diffusional hindrance inside the pores, controlling the process. To support this idea, the adsorption rate and the intraparticle diffusion rate for our system were compared by means of the Thiele modulus (h) [44]. A value of $h^2 = 10^{-7}$ was obtained, expressing that the intraparticle diffusion rate exceeds the adsorption rate by

Author's personal copy

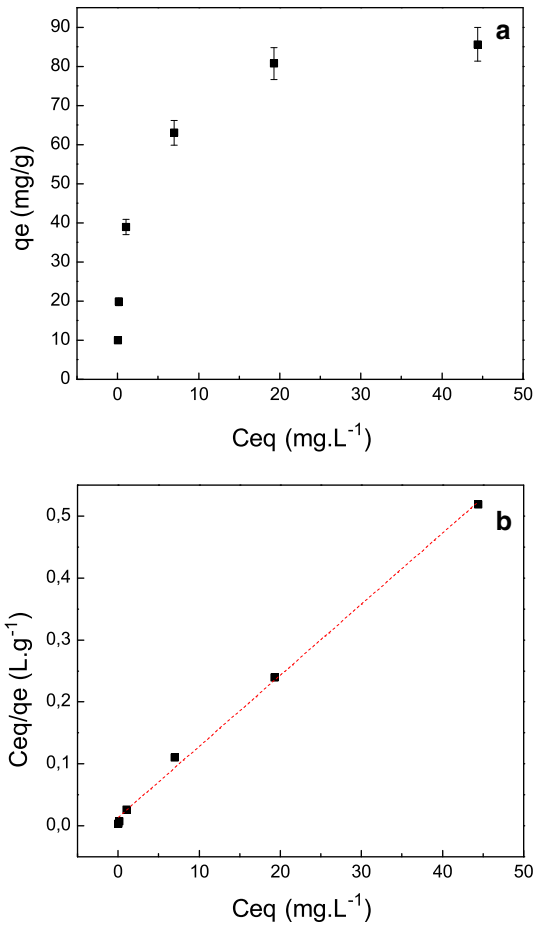

Fig. 10 **a** Adsorption isotherm obtained at constant pH (2.2), T = 25 °C for Cr(VI) on MSSP-APSw from experiments performed in 25 mL solution containing initially chromium concentration in the range 10–130 ppm, **b** linearization of adsorption experimental data using the Langmuir model

about seven orders of magnitude. Thence, it can be affirmed that pore resistance effects are negligible and that the solution bathes the whole pore volume with a uniform concentration of Cr(VI). Details of this calculation are shown in Supporting Information Section.

Therefore, the results indicate that the solid MSSP-APSw exhibits a very high adsorption capacity for aqueous Cr(VI) compared to other absorbents.

3.3 Reutilization and stability of mesoporous hybrid material

As stated in the previous section, MSSP-APSw have high capacity to Cr(VI) removal from water. However, it is very important to evaluate the possibility of degradation of the material under operation conditions, which is essential for their reusability and thus for their long-term application.

As was described, the MSSP-APSw sample was used in chromium adsorption experiments at pH = 2.2 and 10 ppm

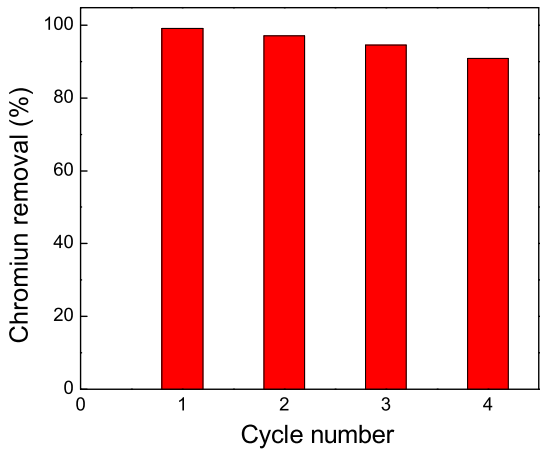

Fig. 11 Variation of the chromium sorption capacity of MSSP-APSw measured at pH = 2.2, 25 °C and Cr(VI) 10 ppm (adsorbent/Cr(VI) solution ratio equal to 1 mg mL^{-1}), for four successive experiments after desorption between them in 10^{-6} M NaOH for 60 min (adsorbent/basic solution ratio equal 1 mg mL^{-1})

chromium concentration (reaching 100 % removal when used for the first time). After filtrate, and in order to desorb the adsorbed chromium, the used sample was suspended in basic solution (NaOH, pH 8) with an adsorbent/solution ratio equal to 1 mg mL^{-1}, stirred for 60 min and separated by filtration. This adsorption/desorption cycle was repeated four times. A slightly decreasing tendency is observed, but in all the cases, the adsorbed chromium percentage is up to 90 % (Fig. 11).

It is well known that silica matrices containing amino functions can suffer from dissolution at the pore surface and subsequent leaching of the organic functions. This reaction is faster when pH increases due to the basic properties of $–NH_2$ functions that attack the Si–O–Si network. For MSSP-APSw sample after 240 min in basic medium (NaOH, pH 8) 6.5 % of amino leaching was registered. This small fraction of the aminopropylsilane groups would be lost, in the same way, in the chromium desorption procedures and could explain the slight decrease in Cr(VI) adsorption depicted in Fig. 11.

4 Conclusions

Ordered mesoporous silica spherical particles, whose surface was modified with anchored aminopropyl groups, were synthesized. It was demonstrated that a post-synthesis surface modification under mild reaction conditions (6 h, T = 80 °C) does not alter the initial mesoporous structure. The incorporation of amino groups provides to the solid a good capacity and a rapid kinetic towards adsorption of Cr(VI) in aqueous medium. The behavior of the organic/inorganic hybrid material as adsorbent is highly affected by

Author's personal copy

pH. The maximum adsorption capacity of Cr(VI) is attained at controlled pH between 2 and 3, due to the fact that at higher pH the deprotonation of both, amino and Si–OH surface groups occurs. As a consequence chromate anions will appear, leading to an adsorbent/adsorbate repulsion, which makes the adsorption process be less efficient. The maximum adsorption capacity, 87.1 mg of Cr(VI) per gram of solid at pH = 2.2, was determined applying the Langmuir monolayer model. This high q_{max} value compared with other hybrid mesoporous silica adsorbents might arise from the narrow particle size distribution, with nanometric particles, which results in a high accessibility of the adsorbate species at active sites located deep inside the adsorbent framework and the absence of diffusional restrictions within the pores. Therefore, there is not a profile concentration inside the particles and the process is controlled by the adsorption kinetic. It is remarkable that the amino grafted functions are stable during use and regeneration, giving the hybrid material long term stability and reusability. The results reported in the present work indicate that the obtained material could be used as adsorbent for the separation/recuperation of aqueous Cr(VI).

Acknowledgments This work was funded by Universidad Nacional de Río Negro (UNRN) (PI-40-C-161) and Comisión Investigaciones Científicas de la Provincia de Buenos Aires (CICPBA). PPM thank Consejo Nacional de Investigaciones Científicas y Técnicas (CONICET) for a graduate student fellowship. NAF and SGM are CONICET staff researchers. JFB is CICPBA staff researcher. Authors would like to thank Dr. I. Lick for her assistance in TGA measurements and Dr. S. P. Bressa for his assistance in diffusional criteria analysis.

References

1. P. Misaelides, Micropor. Mesopor. Mat. **144**, 15–18 (2011)
2. S. Goubert-Renaudin, M. Etienne, S. Brandes, M. Meyer, F. Denat, B. Lebeau, A. Walcarius, Langmuir **25**, 9804–9813 (2009)
3. W. Yang, P. Ding, L. Zhou, J. Yu, X. Chen, F. Jiao, App. Surf. Sci. **282**, 38–45 (2013)
4. D.A. White, R.L. Bussey, Sep. Pur. Tech. **11**, 137–141 (1997)
5. L.C.A. Oliveira, D.I. Petkowicz, A. Smaniotto, S.B.C. Pergher, Water Res. **38**, 3699–3704 (2004)
6. C. Luengo, V. Puccia, M. Avena, J. Haz. Mat. **186**, 1713–1719 (2011)
7. Y. Li, B. Gao, T. Wu, D. Sun, X. Li, B. Wang, F. Lu, Water Res. **43**, 3067–3075 (2009)
8. P. Wang, I.M.C. Lo, Water Res. **43**, 3727–3734 (2009)
9. S. Chen, Q. Yue, B. Gao, Q. Li, X. Xu, Chem. Eng. J. **168**, 909–917 (2011)
10. J. Febrianto, A.N. Kosasiha, J. Sunarso, Y. Ju, N. Indraswati, S. Ismadji, J. Haz. Mat. **162**, 616–645 (2009)
11. Y. Li, S. Zhu, Q. Liu, Z. Chen, J. Gu, C. Zhu, T. Lu, D. Zhang, J. Ma, Water Res. **47**, 4188–4197 (2013)
12. J. Wang, S. Zheng, Y. Shao, J. Liu, Z. Xu, D. Zhu, J. Col. Inter. Sc. **349**, 293–299 (2010)
13. H. Yoshitake, J. Mater. Chem. **20**, 4537–4550 (2010)
14. C.T. Kresge, M.E. Leonowicz, W.J. Roth, J.C. Vartulli, J.S. Beck, Nature **359**, 710–712 (1992)
15. F. Raji, M. Pakizeh, App. Surf. Sci. **282**, 415–424 (2013)
16. S. Angelos, M. Liong, E. Choi, J.I. Zink, Chem. Eng. J. **137**, 4–13 (2008)
17. D. Pérez-Quintanilla, I. Sierra, J. Porous Mater. **21**, 71–80 (2014)
18. A. Calvo, P.C. Angelomé, V.M. Sánchez, D.A. Scherlis, F.J. Williams, G.J.A.A. Soler-Illia, Chem. Mater. **20**, 4661–4668 (2008)
19. L. Mercier, T.J. Pinnavaia, Environ. Sci. Technol. **32**, 2749–2754 (1998)
20. M.V. Lombardo, M. Videla, A. Calvo, F.G. Requejo, G.J.A.A. Soler-Illia, J. Haz. Mat. **223–224**, 53–62 (2012)
21. N. Velikova, Y. Vueva, Y. Ivanova, I. Salvado, M. Fernandes, P. Vassileva, R. Georgieva, A. Detcheva, J. of Non-Crys. Sol. **378**, 89–95 (2013)
22. J. Cao, Y. Wub, Y. Jin, P. Yilihan, W. Huang, J. Taiwan Inst. Chem. Eng. **45**, 860–868 (2014)
23. T. Yokoi, T. Tatsumi, H. Yoshitake, J. Coll. Inter. Sci. **274**, 451–457 (2004)
24. A. Walcarius, M. Etienne, B. Lebeau, Chem. Mater. **15**, 2161–2173 (2003)
25. A. Szegedi, M. Popova, I. Goshev, J. Mihály, J. Solid State Chem. **184**, 1201–1207 (2011)
26. N.K. Renuka, A.K. Praveen, K. Anas, Mater. Lett. **109**, 70–73 (2013)
27. M. Grün, K.K. Unger, A. Matsumoto, K. Tsutsumi, Micropor. Mesopor. Mater. **27**, 207–216 (1998)
28. J. Villarroel-Rocha, D. Barrera, K. Sapag, Top. Catal. **54**, 121–134 (2011)
29. APHA, *Standard methods for the examination of water and wastewater*, 16th edn. (Washington, DC, 1985)
30. M. Etienne, A. Walcarius, Talanta **59**, 1173–1188 (2003)
31. A. Szegedi, M. Popova, I. Goshev, S. Klébert, J. Mihály, J. Solid State Chem. **194**, 257–263 (2012)
32. Q. Yuan, Y. Chi, N. Yu, Y. Zhao, W. Yan, X. Li, B. Dong, Mat. Res. Bull. **49**, 279–284 (2014)
33. J. Wang, S. Zheng, Y. Shao, J. Liu, Z. Xu, D. Zhu, J. Coll. Inter. Sci. **349**, 293–299 (2010)
34. S. Kim, J. Ida, V.V. Guliants, J.Y.S. Lin, J. Phys. Chem. B **109**, 6287–6293 (2005)
35. V. Hernández-Morales, R. Nava, Y.J. Acosta-Silva, S.A. Macías-Sánchez, J.J. Pérez-Bueno, B. Pawelec, Micropor. Mesopor. Mater. **160**, 133–142 (2012)
36. V.R. Elías, M.I. Oliva, S.E. Urreta, S.P. Silvetti, K. Sapag, A.M. Mudarra-Navarro, S.G. Casuscelli, G.A. Eimer, Appl. Catal. A Gen. **381**, 92–100 (2010)
37. J.C. Groen, L.A.A. Peffer, J. Perez-Ramirez, Micropor. Mesopor. Mat. **60**, 1–17 (2003)
38. B.V. Zhmud, J. Sonnefeld, J. Non-Cryst, Sol. **195**, 16–27 (1996)
39. K. Dimos, P. Stathi, M.A. Karakassides, Y. Deligiannakis, Microp. Mesopor. Mat. **126**, 65–71 (2009)
40. V.R. Elías, E.V. Sabre, E.L. Winkler, L. Andrini, F.G. Requejo, S.G. Casuscelli, G.A. Eimer, J. Sol. State Chem. **213**, 229–234 (2014)
41. R.K. Tandon, P.T. Crisp, J. Ellis, Talanta **31**, 227–228 (1984)
42. A. Walcarius, C. Delacóte, Acta **547**, 3–13 (2005)
43. T. Burks, M. Avila, F. Akhtar, M. Göthelid, P.C. Lansåker, M.S. Topraka, M. Muhammed, A. Uheida, J. Colloid Interface Sci. **425**, 36–43 (2014)
44. R. Aris, *Introduction to the Analysis of Chemical Reactors* (Prentice-Hall Inc, Englewood Cliffs, 1965)